Effects of structural heterogeneity of nanostructured copper on the evolution of the sizes of recrystallized grains during annealing

Lin, Fengxiang; Zhang, Yubin; Pantleon, Wolfgang; Juul Jensen, Dorte

Published in:
I O P Conference Series: Materials Science and Engineering

Link to article, DOI:
10.1088/1757-899X/89/1/012033

Publication date:
2015

Document Version
Publisher's PDF, also known as Version of record

Effects of structural heterogeneity of nanostructured copper on the evolution of the sizes of recrystallized grains during annealing

2015 IOP Conf. Ser.: Mater. Sci. Eng. 89 012033

(http://iopscience.iop.org/1757-899X/89/1/012033)

Effects of structural heterogeneity of nanostructured copper on the evolution of the sizes of recrystallized grains during annealing

F X Lin[1], Y B Zhang[1], W Pantleon[2] and D Juul Jensen[1]
[1]Danish-Chinese Center for Nanometals, Section for Materials Science and Advanced Characterization, Department of Wind Energy, Technical University of Denmark, Risø Campus, 4000 Roskilde, Denmark
[2]Section for Materials and Surface Engineering, Department of Mechanical Engineering, Technical University of Denmark, 2800 Kongens Lyngby, Denmark

E-mail: lnfe@dtu.dk

Abstract. Recrystallization in copper deformed by dynamic plastic deformation was investigated using electron backscatter diffraction. The recrystallized grains show a broad size distribution. The kinetics of grains of different sizes is observed to be different: In the beginning of recrystallization, the area fraction of small recrystallized grains increases rapidly. At later stages of recrystallization, the area fraction of small recrystallized grains is stable, while the area fractions of medium and large recrystallized grains increase. Correlation between the broad grain size distribution (and its evolution) and the heterogeneous deformed microstructure is discussed.

1. Introduction

After deformation at cryogenic temperatures or with high strain rates, copper often has different mechanical properties, textures and microstructures, compared with room temperature low-strain-rate deformation [1-3]. During low temperature or high-strain-rate deformation, mechanical twinning occurs, depending on the crystallographic orientations of the grains [4]. Nano-sized mechanical twins have been reported to favour the formation of shear bands [5]. Both mechanical twins and shear bands increase the structural heterogeneity of the deformed sample, which affects subsequent annealing behaviour. In earlier work, we studied copper deformed in liquid nitrogen by dynamic plastic deformation (DPD) with strain rates in the range of 10^2-10^3 s^{-1}, and found that the structural heterogeneity significantly affected the recrystallization kinetics [6]. In the present work, we investigate the correlation between the structural heterogeneity of the deformed sample and the recrystallized microstructure.

2. Experimental

A cylindrical copper sample (99.995% purity) with an initial grain size of 200 μm was immersed in liquid nitrogen and deformed by DPD to a strain of 2.1 ($\varepsilon = \ln(L_0/L_f)$, where L_0 and L_f are the sample height before and after deformation, respectively). The samples were deformed at Institute of Metal Research, Shenyang, China, transported to Denmark, and kept at -18 °C for a few months. A volume

fraction of around 18% was already recrystallized before we started the present investigation and conducted furnace annealing [6]. This initial partial recrystallization has to be considered in the analysis of the present results, but is not expected to affect the conclusions reached.

The samples were isothermally annealed at 120 °C for time intervals from 2 minutes to 4 h to achieve various recrystallized volume fractions. Cross sections of the samples were ground and electro-polished using a D2 electrolyte. Microstructures of the cross section were characterized using electron backscatter diffraction (EBSD) with a step size of 0.5 µm, and for each annealing time, two to seven maps with a typical size of 250 × 300 µm^2 each were obtained. For the sample annealed for 5 minutes, three extra scans over relatively large regions (~1000 × 300 µm^2 each) using a step size of 1 µm were conducted, in order to reveal the sample heterogeneity on a larger scale. Also for the sample annealed for 5 minutes, an extra specimen was prepared by mechanical polishing of the cross section using 40 nm oxide polishing suspension to obtain a better surface quality for a better characterization of the deformed matrix.

The in-house code DRG was applied to identify recrystallized grains [7]. The recrystallized grains were defined as grains with internal misorientations less than 1°, fully or partly surrounded by high angle boundaries, with misorientation angles larger than 15°, and with a grain size larger than a critical value. The proper critical grain size is affected by the scanning step size. In this work, an equivalent circular diameter (ECD) of 3 µm and 1.5 µm was chosen as the critical size for maps scanned with a step size of 1 µm and 0.5 µm, respectively. During detection of recrystallized grains, twin boundaries were ignored; thus annealing twins and the parent grain are treated as one grain.

3. Results and discussion

3.1. Partially recrystallized microstructure

Figure 1 shows the recrystallized part of the sample after 5 minutes of annealing in a relatively large sample area (1380 × 300 µm^2) scanned with a step size of 1 µm. The area shown in figure 1 is 39% recrystallized. When 3 maps of sizes comparable to figure 1 are averaged, the sample was found 34% recrystallized. Recrystallized grains tend to form bands almost perpendicular to the compression axis, with band widths from a few µm to more than 200 µm. In general, the spatial distribution of the recrystallized grains is very heterogeneous.

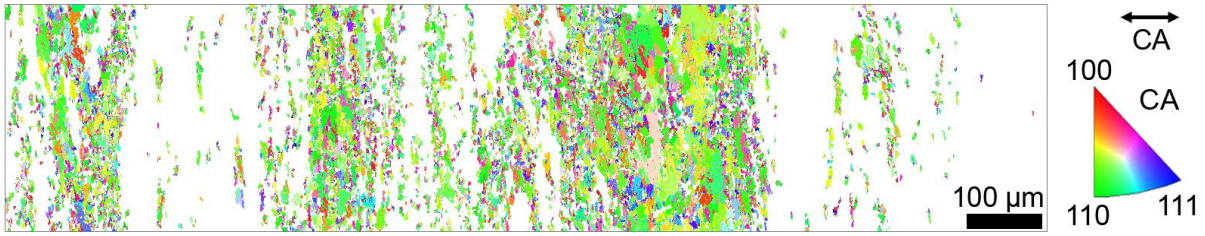

Figure 1. Orientation map showing the recrystallized grains in the sample annealed for 5 minutes. The compression axis (CA) is horizontal. The white regions are unrecrystallized, and other colours represent the crystallographic direction of the recrystallized grains along CA.

In the sample annealed for 5 minutes, the recrystallized grains show a broad grain size distribution. The number weighted average ECD of recrystallized grains is 6.6 µm, whereas the maximum ECD is 60 µm, about 9 times the average grain size. The size distribution of recrystallized grains is plotted in figure 2 using both number and area weighted density functions, f_N and f_A:

$$f_N(D_i) = \frac{F_N(D_i)}{\Delta D_i} \quad (1)$$

$$f_A(D_i) = \frac{F_A(D_i)}{\Delta D_i} \quad (2)$$

where $F_N(D_i)$ and $F_A(D_i)$ are the number and area fractions, respectively, and ΔD_i is the bin size, which is 1 μm for figure 2. In the number density plot, only one peak appears, since the number of small grains is much larger than that of large grains. In the area density plot, a long tail is clearly seen for grains larger than 20 μm.

A lognormal distribution is usually observed for the grain sizes after recrystallization [8]. For this sample, lognormal functions were used to fit f_N and f_A (figure 2). For the number density distribution, significant deviations from the lognormal function appear at around 10 μm and above. Clearly, the sizes of the recrystallized grains in this sample do not follow the lognormal distribution. On the other hand, a reasonable description of the area density distribution can be achieved by a lognormal distribution.

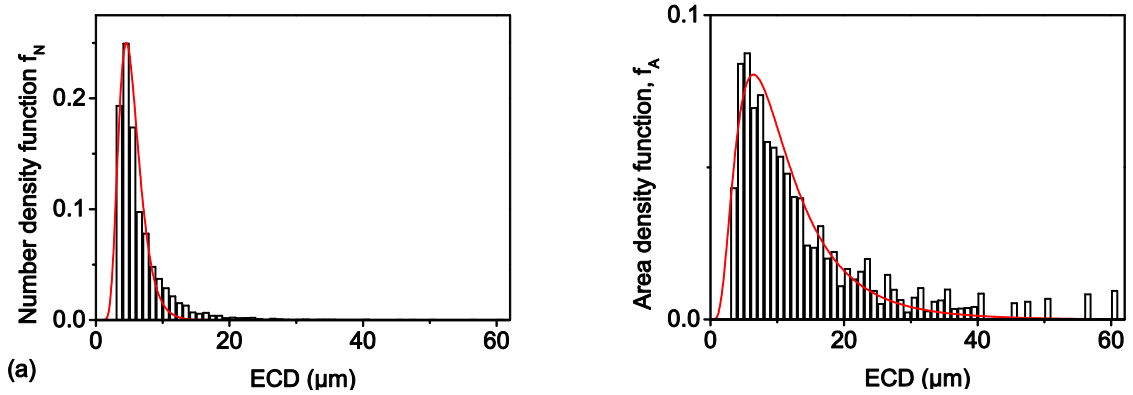

Figure 2. Number (a) and area (b) weighted grain size density functions for recrystallized grains in the sample annealed for 5 minutes. Lognormal functions were used to fit the density functions, which are shown by the red lines.

To analyse possible differences between grains of different sizes, the recrystallized grains are divided into three groups: small grains (ECD < 10 μm), medium grains (10 μm ≤ ECD < 20 μm), and large grains (ECD ≥ 20 μm). The three groups of grains in figure 1 are shown separately in figure 3. The large grains are severely clustered, and most of them are located along three bands. It is noted that the locations of these large grains correspond to the three thickest bands (>100 μm wide) in figure 1. The small grains tend to form thin bands, which are a few to tens of μm wide. The spatial distribution of small grains is more dispersed than that of the medium and large ones, but clearly not homogeneous: there are several locations, where thin bands cluster to form thicker ones, and several other locations, where recrystallized grains are rarely observed in bands of 50 μm to 200 μm wide.

As shown by the inverse pole figures corresponding to the compression axis (figure 3), the recrystallized grains show a weak fibre texture for all the three groups of grains with the maximum intensity shifted from <110> towards <100>. The orientations of the large grains are not significantly different from those of the small grains. This result can be compared to a heavily cold-rolled and annealed copper sample with an initial grain size of 22 μm, in which a broad size distribution is also observed [9]. In that sample, it has been shown that the large grains are all cube oriented grains, whereas small grains have various orientations [9]. Different to the rolled sample, the large sizes of a few grains in the present sample are not associated with a special orientation different from that of the small grains. It is rather suggested that the formation of large grains in the present sample strongly depends on the local deformed microstructure, as evidenced by the severe clustering.

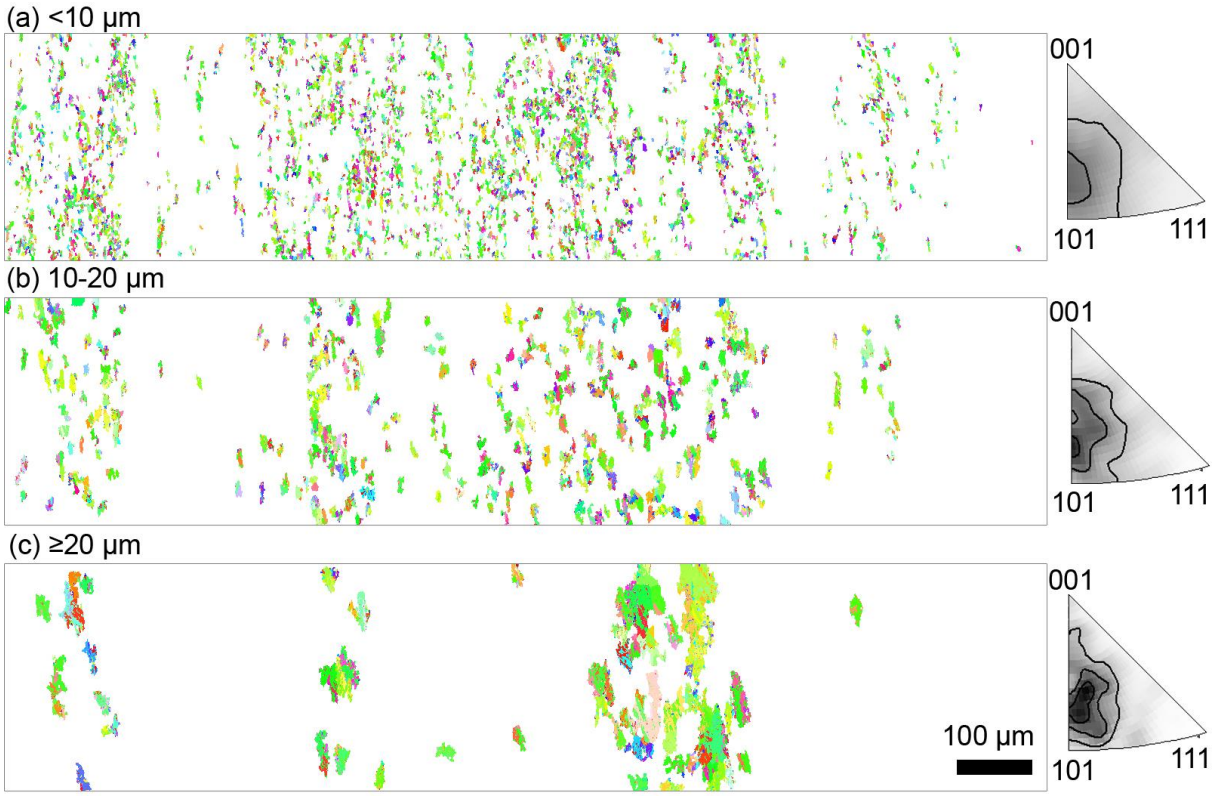

Figure 3. Orientation maps and inverse pole figures (IPFs, corresponding to CA) of the recrystallized grains belonging to different size groups in the sample annealed for 5 minutes (same as figure 1): (a) ECD < 10 µm, (b) 10 µm ≤ ECD < 20 µm, (c) ECD ≥ 20 µm. It should be noted that twin boundaries were ignored when defining grains. Thus a single grain in the map often has several parts with different colours. Contour levels in the IPFs are multiples (1, 2, 3) of random intensity.

3.2. Kinetics

The area fractions of recrystallized grains belonging to the three size groups are plotted in figure 4 as a function of annealing time. The sample without furnace annealing was already 18% recrystallized, and the recrystallized parts contain almost equal area fractions of small, medium and large grains. During furnace annealing, the area fraction of small grains increases with annealing time until approximately 30 minutes. After 30 minutes, the area fraction of small grains tends to be stable, and accounts for around 40% of the characterized area. The area fraction of medium grains increases slowly until 1 h, but from 1 h to 4 h the area fraction of medium grains doubles. Similarly, the area fraction of large grains is almost stable up to 1 h, but increases from 1 h to 4 h.

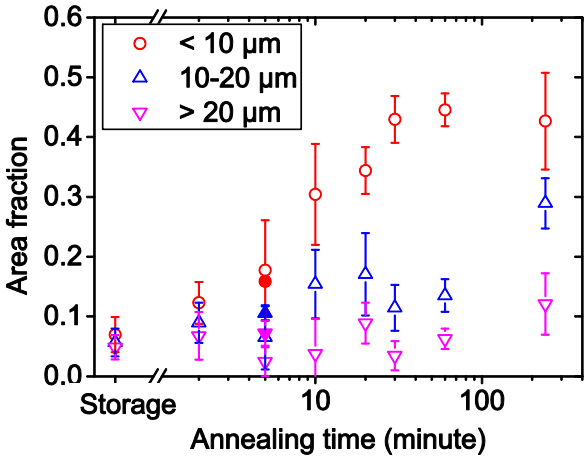

Figure 4. Evolution of area fraction of different sized recrystallized grains as a function of annealing time, determined based on EBSD maps scanned with a step size of 0.5 μm. For the sample annealed for 5 minutes, an extra set of data, shown with solid marks, was determined from larger EBSD maps scanned with a step size of 1 μm (the same EBSD data as used in Section 3.1). The error bars show the standard errors.

3.3. Correlation with the heterogeneity of the deformed microstructure

Based on our previous EBSD characterization (step size 50 nm) of the same DPD sample prepared by electropolishing, the deformed microstructure of the DPD sample was found to consist of three types of regions [6]. Type A regions belong to a <110> fibre texture, and contain mainly low angle boundaries. Type B regions belong to a <111> fibre texture, and consist of nanoscale twins. Type C regions could not be indexed. In the present work, the surface quality was improved using mechanical polishing, after which Type C regions can also be indexed when a small step size was used. The map shown in Figure 5a illustrates this and contains all three types of microstructures. The green region in the left part of figure 5a is a typical Type A structure, while the blue region in the right part is a typical Type B region with twins. Type C regions are marked with blue borders in figure 5b, and they are bands with a width less than 3 μm, containing very fine structures. According to the morphology, most of the Type C regions in figure 5b are shear bands, like those observed by transmission electron microscopy (TEM) [10]. These shear bands cluster in the centre of figure 5b. It should be noted that figure 5 only covers a small region, and Type C regions in fact include not only shear bands, but also other regions of very fine structures, such as fragmented twins.

When a larger scanning step size is used, the indexed ratio decreases significantly even with a good surface quality, as shown in figure 5c. Type A and B regions can still be relatively well indexed, although the internal microstructures are not resolved. Most of the non-indexed points correspond to Type C regions, but some parts of Type B regions are not indexed either, most likely because of an overlap of EBSD patterns. As an approximation, it is possible to determine area fractions of the three types of deformed microstructures from EBSD maps scanned with a relatively large step size based on the different orientations, although this method tends to underestimate the amount of Type B regions.

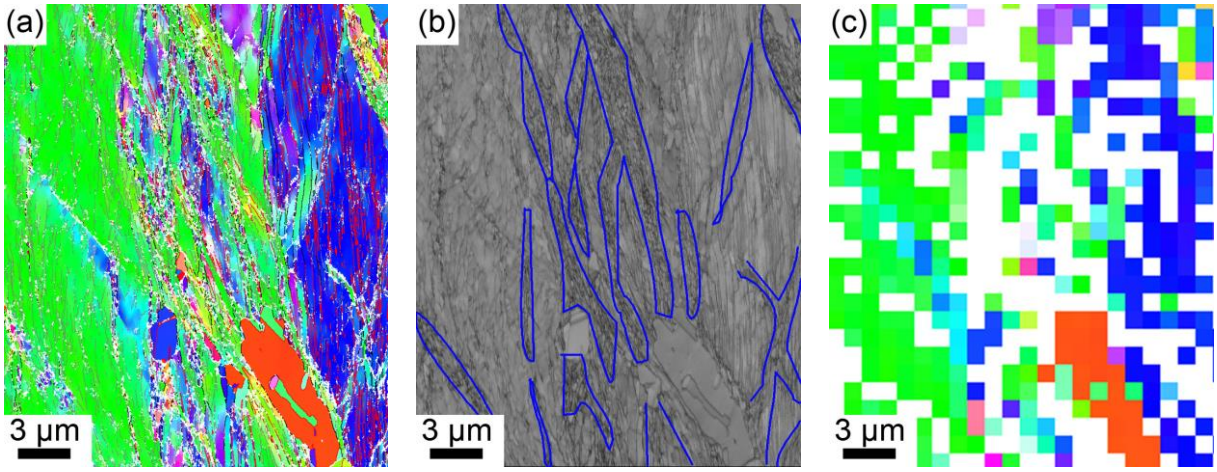

Figure 5. Orientation maps of a small region in the sample annealed for 5 minutes, with a surface prepared by mechanical polishing. CA is along the horizontal direction. Maps (a) and (b) are from the same EBSD data scanned with a step size of 30 nm, and Map (c) is the same area but scanned with a step size of 1 µm. The colours in (a) and (c) represent the crystallographic direction along CA, and the white regions are non-indexed points. Black, grey and red lines in (a) represent boundaries with misorientations higher than 15° and 2°, and twin boundaries, respectively. Map (b) shows the band contrast (BC). Regions in (b) bounded by blue lines indicate regions with a very fine structure. Note that these fine-structure regions correspond approximately to the non-indexed regions in Map (c).

Figure 6 shows the deformed microstructure on a larger scale. The map was obtained also with a coarse step size of 0.5 µm, and thus contains a relatively large area fraction of non-indexed points. The indexed parts mainly belong to a <110> fibre texture (green colour), and some parts belong to a <111> fibre texture (blue colour). Very few isolated points that belong to <100> fibre texture (red colour) are also observed. As discussed above, regions with a <110> and <111> texture are considered as Type A and B, respectively. All the non-indexed points are considered as Type C. The few isolated <100> texture points are also grouped into Type C regions.

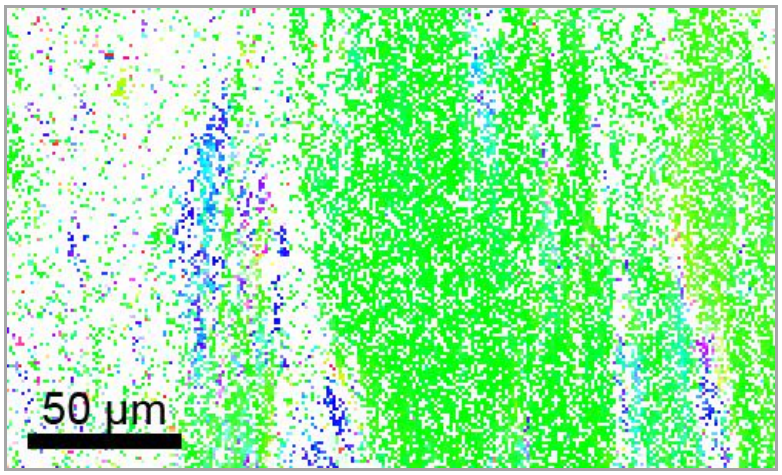

Figure 6. Orientation map obtained with a step size of 0.5 µm, showing the deformed microstructure in the sample without furnace annealing. CA is horizontal. White points are non-indexed, and other colours represent the crystallographic direction along CA. The microstructure is divided into three types according to the local orientations. Type A: <110> texture, Type B: <111> texture, Type C: non-indexed points and the few isolated <100> oriented points.

Figure 7 shows the area fractions of the three types of deformed microstructures determined this way in samples annealed for different time periods. In the sample without furnace annealing, the area fractions of Type A and C regions are similar, and are around 40% each. The area fraction of Type C regions decreases quickly during furnace annealing, whereas the area fraction of Type A regions decreases much more slowly. After 1 h annealing, when the sample is 64% recrystallized, only few Type C regions are left, but there is still an area fraction of around 30% of Type A regions. The area fraction of Type B regions is about 5% in the sample without furnace annealing. Considering the small amount of Type B regions, they do not significantly affect the recrystallization process, and will not be discussed further.

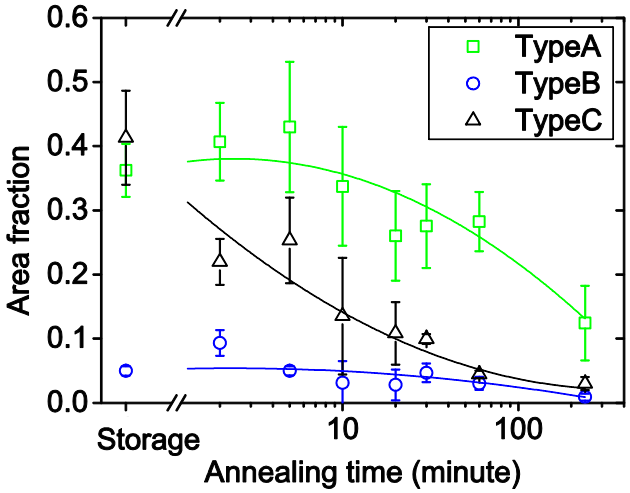

Figure 7. Evolution of area fraction of the three types of deformed microstructures as a function of annealing time, determined based on EBSD data obtained with a step size of 0.5 μm. Type A/B/C regions were determined according to the local orientations, as demonstrated in figure 6. The error bars show the standard errors. Second order polynomial functions were fitted to the data points, shown by the curves, to clearly visualize the trends for the different types of deformed microstructures.

The decrease in area fractions of Type C and Type A regions is due to recrystallized grains nucleating and growing in the these regions. One may speculate whether previous non-indexed regions become indexed after annealing, namely Type C regions being erroneously treated as other types. But it would require significant recovery, which has not been observed by TEM in a similar material [11]. By comparing figures 4 and 7, it is seen that before 30 minutes, the major area decrease in the deformed matrix occurs in Type C regions, and at the same time, the area fraction of small recrystallized grains increases. After 1 h, few Type C regions are left, and the area fraction of small recrystallized grains stabilizes. These two observations suggest that most of the small recrystallized grains form in Type C regions, and are limited to this type of regions and do not grow into the neighbouring Type A/B regions. As Type C regions have a very fine structure, and thus also high stored energy [12], the nucleation density is high in this type of regions. Recrystallized grains will thus quickly impinge, resulting in a small recrystallized grain size. These interpretations are supported by the fact that the area fraction of small recrystallized grains is close to that of Type C regions after storage.

From 1 h to 4 h, the increase in the recrystallized area is mostly by growth of medium and large recrystallized grains. At the same time, the area fraction of Type A regions decreases in the deformed matrix. The Type A regions are thus likely to be the places where medium and large recrystallized grains develop. The internal microstructure of Type A regions contains only low angle boundaries, and thus Type A regions may have only a few nucleation sites. Therefore, Type A regions are more likely

to develop grains of larger sizes. The stored energy of Type A regions is also lower compared with Type C regions, and the recrystallization kinetics is thus slower.

As shown in figure 4, the area fraction of large grains is more or less constant before 1 h. This means that possibly most of the large grains observed in the beginning of recrystallization, such as those shown in figure 3c, form during the storage. Whether a fresh deformed sample will also behave like this or the phenomenon only occurs during long-term low temperature storage needs further investigations.

4. Conclusions

We investigated recrystallization in copper deformed by DPD using EBSD. The deformed sample contains three types of microstructure: Type A with a {110} fibre texture, Type B with twins and Type C with very fine structures. In the sample without furnace annealing, similar area fractions of Type A and C regions are observed, while the area fraction of Type B regions is very small. The recrystallized grains were found to have a broad size distribution. The sizes of grains are not related to the orientations of the recrystallized grains, but to the deformed matrix where the recrystallized grains grow. The area fraction of small recrystallized grains (< 10 μm) increases rapidly from the beginning of recrystallization, and saturates at later stages of recrystallization. The small recrystallized grains are considered to develop mainly in Type C regions. At the later stages of recrystallization, medium (10–20 μm) and large (> 20 μm) recrystallized grains still increase, and they are considered to develop at Type A regions.

Acknowledgements

The authors are grateful to Drs N. Hansen and N.R. Tao for helpful discussions, Mr. X. Si for DPD sample preparation at IMR, and Dr. G.H. Fan for help with mechanical polishing. The authors gratefully acknowledge the support from the Danish National Research Foundation (Grant No. DNRF86-5) and the National Natural Science Foundation of China (Grant No. 51261130091) for the Danish-Chinese Center for Nanometals, within which this work was performed.

References

[1] Leffers T and Ray R K 2009 *Prog. Mater. Sci.* **54** 351
[2] Bhattacharyya A, Rittel D and Ravichandra G 2005 *Scr. Mater.* **52** 657
[3] Luo Z P, Mishin O V, Zhang Y B, Zhang H W and Lu K 2012 *Scr. Mater.* **66** 355
[4] Hong C S, Tao N R, Lu K and Huang X 2009 *Scr. Mater.* **61** 289
[5] Morri K, Meching H and Nakayama Y 1985 *Acta Mater.* **33** 379
[6] Lin F X, Zhang Y B, Tao N R, Pantleon W and Juul Jensen D 2014 *Acta Mater.* **72** 252
[7] Wu G L and Juul Jensen D 2008 *Mater. Charact.* **59** 794
[8] Pande C S 2000 *Proc. 21st Risø Inter. Symposium on Mater. Sci.* pp 491
[9] Lin F X, Zhang Y B, Pantleon W and Juul Jensen D submitted
[10] Li Y S, Tao N R and Lu K 2008 *Acta Mater* **56** 230
[11] Li Y S, Zhang Y, Tao N R and Lu K 2008 *Scr. Mater.* **59** 475
[12] Yan F and Zhang H W 2012 *J Mater. Sci. Technol.* **28** 289